CEND-2863-217

JOINT U.S.-EURATOM

EUR/AEC Report 1191

JOINT UNITED STATES
ATOMIC ENERGY COMMISSION
RESEARCH AND DEVELOPMENT PROGRAM

PROGRESS REPORT

THE DEVELOPMENT AND TESTING OF UO_2 FUEL SYSTEMS FOR WATER REACTOR APPLICATIONS

Period
April 1 to July 31, 1964

Issued August 1964

NUCLEAR DIVISION
COMBUSTION ENGINEERING, INC.

DISCLAIMER

GEND-2863-217

JOINT U.S.-EURATOM

JOINT UNITED STATES

LEGAL NOTICE

CEND-2863-217
Joint U. S. -Euratom
UC-25, Metals, Ceramics
and Materials
TID-4500, 29th Edition

PROGRESS REPORT

THE DEVELOPMENT AND TESTING OF UO_2 FUEL SYSTEMS FOR WATER REACTOR APPLICATIONS

Period
April 1 to July 31, 1964

Prepared by:

W. P. Chernock
C. E. Burdg
E. I. Veil
G. Zuromsky
J. J. Koziol

Contract AT(30-1)-2863
U. S. Atomic Energy Commission

Issued August 1964

Unclassified
Classification

8/28/64
Authorized Classifier Date

NUCLEAR DIVISION
COMBUSTION ENGINEERING, INC.
WINDSOR, CONNECTICUT

CEND-2863-217
Joint U.S.-Euratom
UC-25, Metals, Ceramics
and Materials
TID-4500, 29th Edition

EXTERNAL DISTRIBUTION:

No. of Copies

Mr. M. Plisner, Contract Administrator — 22
U. S. Atomic Energy Commission
New York Operations Office
376 Hudson Street
New York, New York 10014

Including copies for:

U.S.-Euratom Joint Research and Development Board — 20
51 Rue Belliard
Brussels, Belgium

Mr. J. M. Simmons, Chief — 2
Fuels and Materials Development Branch
U. S. Atomic Energy Commission
Division of Reactor Development
Washington, D. C. 20545

Mr. W. R. Voigt — 3
Water Reactors Branch
U. S. Atomic Energy Commission
Washington, D. C. 20545

Dr. R. C. Dalzell, Assistant Director for Foreign Activities — 2
U. S. Atomic Energy Commission
Division of Reactor Development
Washington, D. C. 20545

U. S. Atomic Energy Commission — 3
Division of Technical Information Extension
Post Office Box 62
Oak Ridge, Tennessee 37831

Mr. Harmon S. Potter, Chief — 1
New York Patent Group
Brookhaven National Laboratory
Upton, L.I., New York 11973

EXTERNAL DISTRIBUTION (Continued):

	No. of Copies
Dr. J. Frye Metallurgy Division Oak Ridge National Laboratory Post Office Box X Oak Ridge, Tennessee	1
Dr. Stephen Lawroski Argonne National Laboratory 9700 South Cass Avenue Argonne, Illinois	4
Mr. T. Pashos General Electric Company Atomic Power Equipment Department Post Office Box 1131 San Jose, California	1
Dr. R. Allio Westinghouse Electric Corporation Atomic Power Department Post Office Box 1075 Pittsburgh, Pennsylvania	1
Dr. Ersel A. Evans General Electric Company Hanford Atomic Products Operation Richland, Washington	1
Mr. L. R. Weissert Babcock and Wilcox Company Research and Development Division Nuclear Development Center Post Office Box 1260 Lynchburg, Virginia	1

CEND-2863-217
Joint U. S. -Euratom
UC-25, Metals, Ceramics
and Materials
TID-4500, 29th Edition

THE DEVELOPMENT AND TESTING OF UO_2 FUEL SYSTEMS FOR WATER REACTOR APPLICATIONS

TABLE OF CONTENTS

CEND-2863-217
Joint U. S. -Euratom
UC-25, Metals, Ceramics
and Materials
TID-4500, 29th Edition

THE DEVELOPMENT AND TESTING OF UO_2 FUEL SYSTEMS FOR WATER REACTOR APPLICATIONS

LIST OF FIGURES

CEND-2863-217
Joint U. S. -Euratom
UC-25, Metals, Ceramics
and Materials
TID-4500, 29th Edition

THE DEVELOPMENT AND TESTING OF UO_2 FUEL SYSTEMS FOR WATER REACTOR APPLICATIONS

LIST OF TABLES

INTRODUCTION

The United States and the European Atomic Energy Community (EURATOM) on May 29 and June 18, 1958, signed an agreement which provides a basis for cooperation in programs for the advancement of the peaceful applications of atomic energy. This agreement, in part, provides for the establishment of a Joint U.S.-Euratom research and development program which is aimed at reactors to be constructed in Europe under the Joint Program.

The work described in this report represents the Joint U.S.-Euratom effort which is in keeping with the spirit of cooperation in contributing to the common good by the sharing of scientific and technical information and minimizing the duplication of effort by the limited pool of technical talent available in Western Europe and the United States.

CEND-2863-217
Joint U. S. -Euratom
UC-25, Metals, Ceramics
and Materials
TID-4500, 29th Edition

THE DEVELOPMENT AND TESTING OF UO_2 FUEL SYSTEMS FOR WATER REACTOR APPLICATIONS

By

W. P. Chernock, C. E. Burdg, E. I. Veil,
G. Zuromsky and J. J. Koziol

ABSTRACT

The thermal conductivity of UO_2 at temperatures up to 2400°C is reported together with an analysis of the temperature for onset of different microstructural constituents. Collapse testing of 3.175 cm diameter tubing with t/R_o values of 0.046 to 0.119 was completed. An analysis of collapse criteria indicates that use of the Tangent Modulus approach provides conservative estimates within 20% of actual collapse pressures within the range of diameters and tube wall thickness tested. Further refinements in the projection welding process have demonstrated dimensional control of tube-to-tube spacings within specified requirements. Tube-to-spacer wire welds are of acceptable metallurgical quality.

I. SUMMARY

Thermal conductivity of UO_2 was determined for temperatures up to 2400°C. A minimum in the conductivity curve was found at 1400°C with values ranging from 0.025 to 0.033 watts/cm-°C. A distinct increase in the thermal conductivity was found for temperatures in excess of 1400°C. The range of values at 2000 and 2400°C are 0.034 to 0.046 and 0.048 to 0.059 watts/cm-°C. Onset of small equiaxed grain growth (with grain diameters greater than 15 μ) was observed at temperatures between 1400 and 1700°C. A difference in radial thermal gradient by a factor of approximately two had little influence on the temperature of onset of small equiaxed grain growth. The onset of massive, blocky grain growth occurred at 2030 to 2190°C and 1940 to 2080°C for the lower and higher radial thermal gradient samples. Although an overlap in the data from these elements is evident, the lower temperatures for onset with the higher radial gradient may be significant.

The collapse test program on 3.175 cm diameter tubing was completed and results have been compared with those previously obtained for smaller diameter tubing. In the range of t/R_o (thickness to radius) and tube diameters tested, the Tangent Modulus Criterion consistently predicted conservative collapse pressures within 20% of the actual values. There appears to be a trend toward better agreement of actual and predicted collapse on the basis of the Inelastic Model at higher t/R_o as the tube diameter increases.

Additional 2-row, 17-tube subassemblies of Type 347 stainless steel were fabricated utilizing improved electrode tooling and fixturing. Tube-to-tube spacings in the two rows of the subassemblies were maintained within

the required range of 1.587 ±0.008 cm (0.625 ±0.003 in.). Lateral displacement or skewing of rows of tubes has been eliminated. However, the diagonal spacings between tubes in the two rows were on the high side of the nominal value of 1.587 cm. A reduction in this spacing dimension will be accomplished by an increase in spacer wire setdown at the weld joints from 0.015 to 0.020 cm (0.006 to 0.008 in.). The control and reproducibility of tube-to-tube dimensions will be demonstrated by the fabrication of a final evaluation subassembly prior to projection welding of the full size 61-tube cluster.

II. THERMAL PERFORMANCE CHARACTERISTICS OF UO_2 - C. E. Burdg, J. J. Koziol

A. Introduction

The objectives of this Task are to determine the thermal conductivity of UO_2, the effective thermal conductivity of a typical fuel element system, and the relationships between microstructure and thermal parameters. Thermal performance testing attempts to simulate, out-of-pile, thermal conditions in a fuel element during irradiation. Successful attainment of these objectives will provide more confidence in UO_2 conductivity values and in the utilization of microstructural analysis as a means of deducing the thermal history of an element.

The last Quarterly Report[1] contained the results of thermal testing of four elements and a composite curve for thermal conductivity which exhibited a distinct upturn at UO_2 temperatures above about 1500°C. A further interesting result was that the "effective conductivity" for the fuel element system did not exhibit significant change when the centerline temperatures were above 500°C; at lower temperatures, the effect of reduced pellet/clad contact pressure resulted in low effective conductivity for the system.

Two compound test elements, consisting of a UO_2 pellet (with its axial heater) surrounded by an insulating sleeve of ZrO_2, were tested to determine the influence of temperature gradient on the system. A third compound element has been prepared but was not tested.

A major effort during this reporting period has been the analysis of thermal and microstructural data with the intent of determining the relationships between microstructure and thermal parameters. This has involved

making detailed measurements on over 250 photomicrographs, and development of interpretative procedures. The results of these analyses are discussed.

B. Test Conditions

1. Run #39

Run #39 was made with a compound element, consisting of a UO_2 pellet surrounded by a ZrO_2 insulating sleeve. As described in the last Quarterly Report[1], the purpose of this configuration was to provide a radial temperature profile which would be significantly different in shape from that existing in a simple all-UO_2 element. Because ZrO_2 has a thermal conductivity of about 0.015 watts/cm-^{o}C, which is only about half that of UO_2, the profile would be expected to be less steep in the UO_2 than in previous tests; the reduction of the gradient is further enhanced by the larger overall diameter of the system. Thus, the effect, if any, of a lower temperature gradient on the microstructure would be demonstrated; and second, the radial position of a given isotherm would be farther from the heater.

Figure 1 shows the compound element configuration, and the sight hole and sectioning plan for element #39. Typical dimensions of the various parts of the compound elements are summarized below:

Component	Material	Dimensions
Clad	Type 304 SS	1.905 cm (0.750 in.) OD x 0.038 cm (0.015 in.) wall
Insulating sleeve	ZrO_2	1.826 cm (0.719 in.) OD x 0.866 cm (0.341 in.) ID
Pellet	UO_2	0.864 cm (0.340 in.) OD x 0.193 cm (0.076 in.) ID
Heater	W-26 Re	0.190 cm (0.075 in.) OD

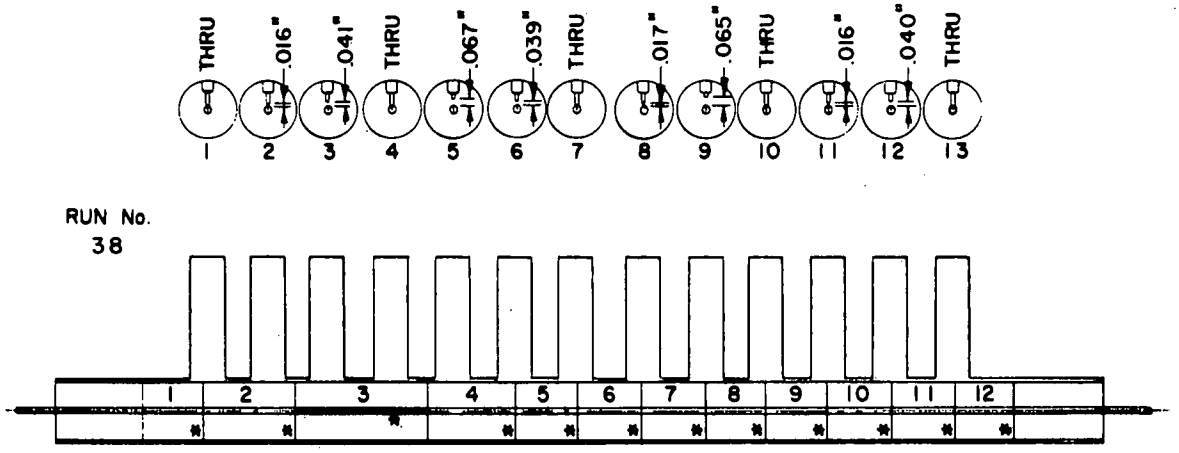

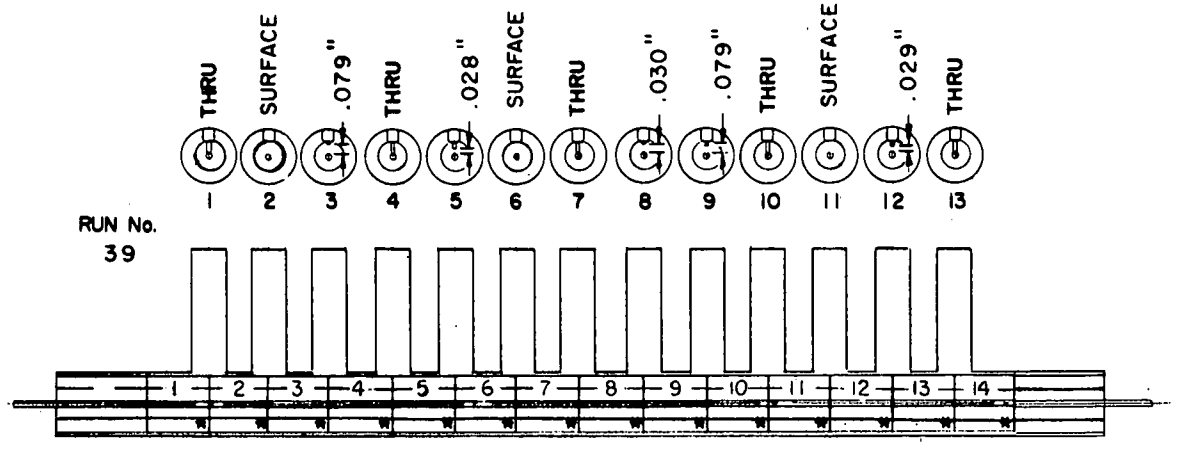

* - THIS SURFACE PREPARED FOR METALLOGRAPHY

SIGHT HOLES AND POST-TEST SECTIONS

Fig. 1

2. Run #40

This run was with an element essentially identical to #39. The run was unsuccessful, in that the axial temperature variation as compared to the temperature variation of the other elements tested was too large to be considered acceptable. An analysis of test conditions failed to establish the cause of this anomalous behavior.

C. Results

1. Thermal Conductivity of UO_2

Knowledge of the behavior of the thermal conductivity of UO_2 as a function of temperature is imperative for the development of a radial temperature distribution for the UO_2 pellets. Having established the temperature variation as a function of radial position in the UO_2, an attempt was made to determine the influence of temperature and thermal gradient on the resulting microstructure.

Thermal conductivity data for sintered polycrystalline UO_2 as a function of temperature up to approximately 1000°C is well documented with close agreement among investigators. Agreement on the findings for conductivity versus temperature above 1000°C is not nearly as good. This is illustrated in the composite curve (Figure 2) constructed from data published by Daniel[2] et al, Godfrey[3] et al, de Halas[4], and Feith[5], along with the CEND data for Runs 38 and 39.

The thermal conductivity curves for runs 38 and 39 result from calculations based on a constant interface gap (between heater and fuel) conductance of 2 watts/cm^2-°C and optical temperature measurements made

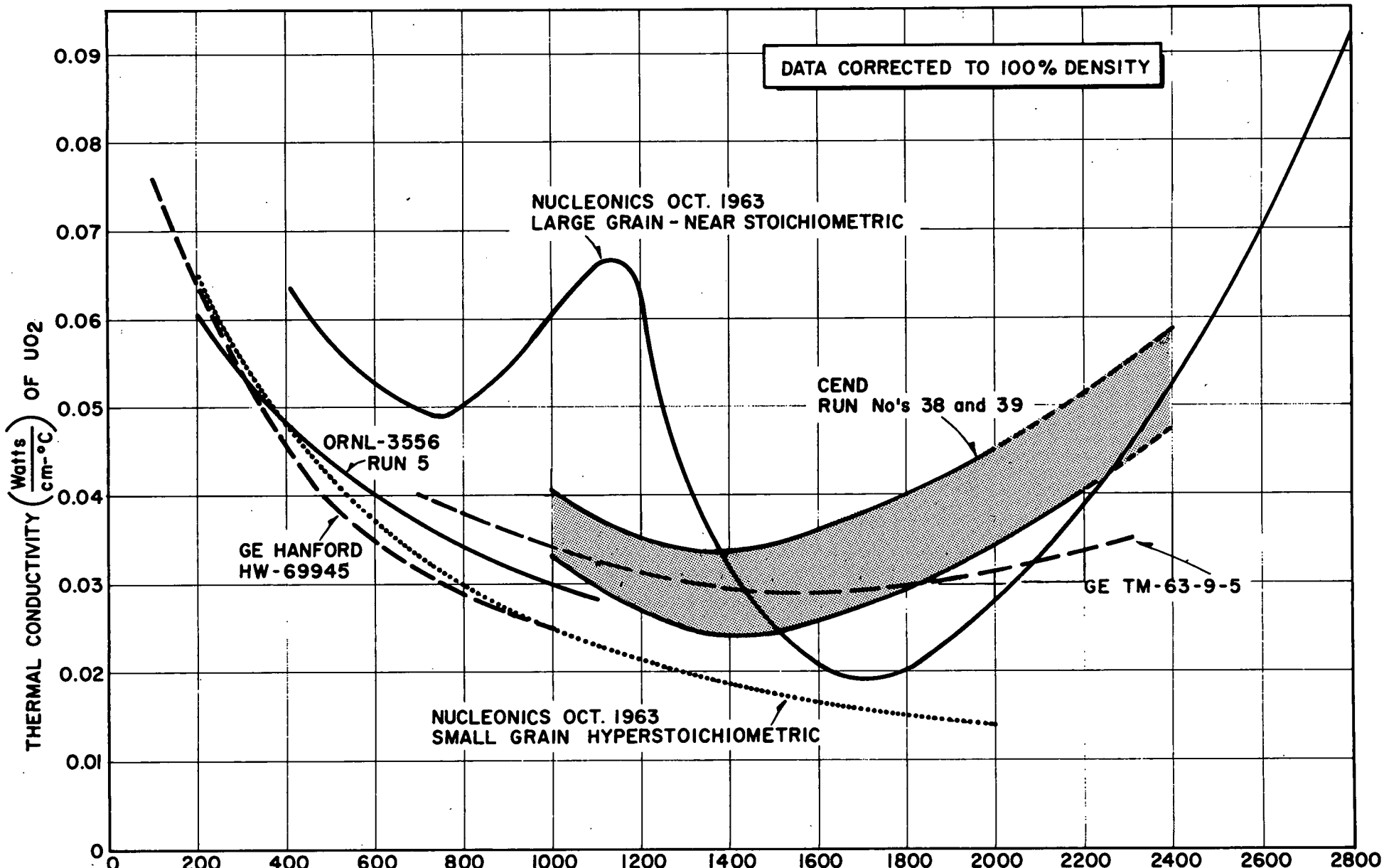

Fig. 2

COMPARISON OF OTHER DATA WITH CEND DATA

by sighting into holes at various radial distances from the heater. The data points obtained from these calculations for runs 38 and 39 fall into the band shown in Figure 2.

This Figure indicates reasonable agreement among investigators at temperatures near 1000°C. At higher temperatures (above 1400°C), CEND's values for the thermal conductivity of UO_2 increase at a greater rate than do the calculated values published by de Halas[4] for small grain hyperstoichiometric UO_2 (no change to positive slope) but do not increase at as great a rate as do the values for large-grain, near-stoichiometric UO_2. The CEND values also increase at a greater rate than do Feith's[5] values which show a minimum at approximately 1600°C.

2. Metallographic Analysis

Elements 38 (uninsulated UO_2 pellets) and 39 (compound element with insulated pellets) were run in the thermal test apparatus for times and temperatures shown in Figure 3. Each element was then sectioned for metallographic examination in accordance with the sectioning plan shown in Figure 1.

Photomacrographs were taken of the entire section to show the post-test appearance of the UO_2 pellet and the tungsten-rhenium heater rod. Photomicrographs were then taken at four positions around the heater rod, 90° apart, as shown in Figure 4.

Analysis of the photomicrographs showed the anticipated large changes in grain size of the UO_2. These changes resulted in the formation, adjacent to the heater rod, of massive grains which, in some instances, were as large as 100 to 200 microns in diameter. Typically, the grains decreased

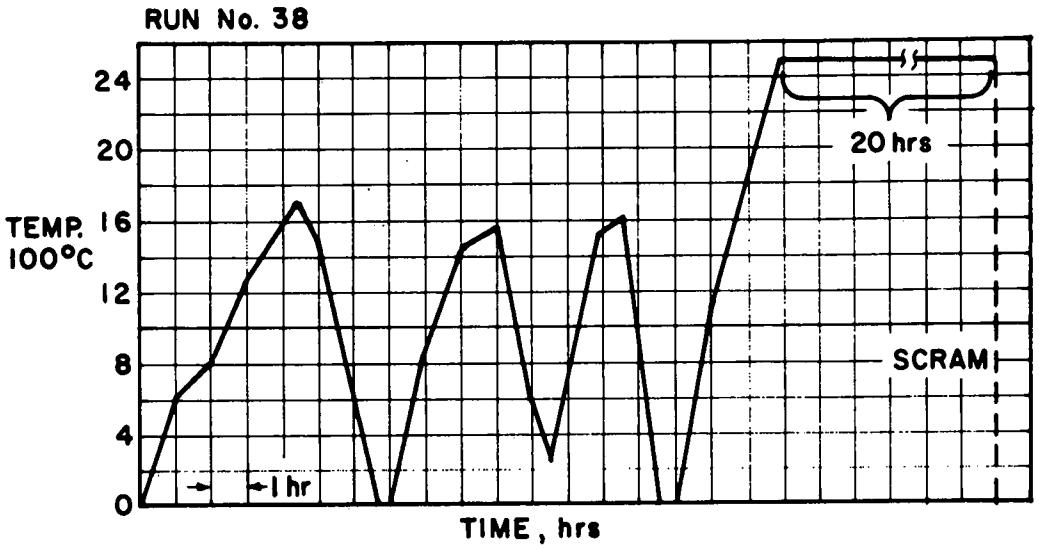

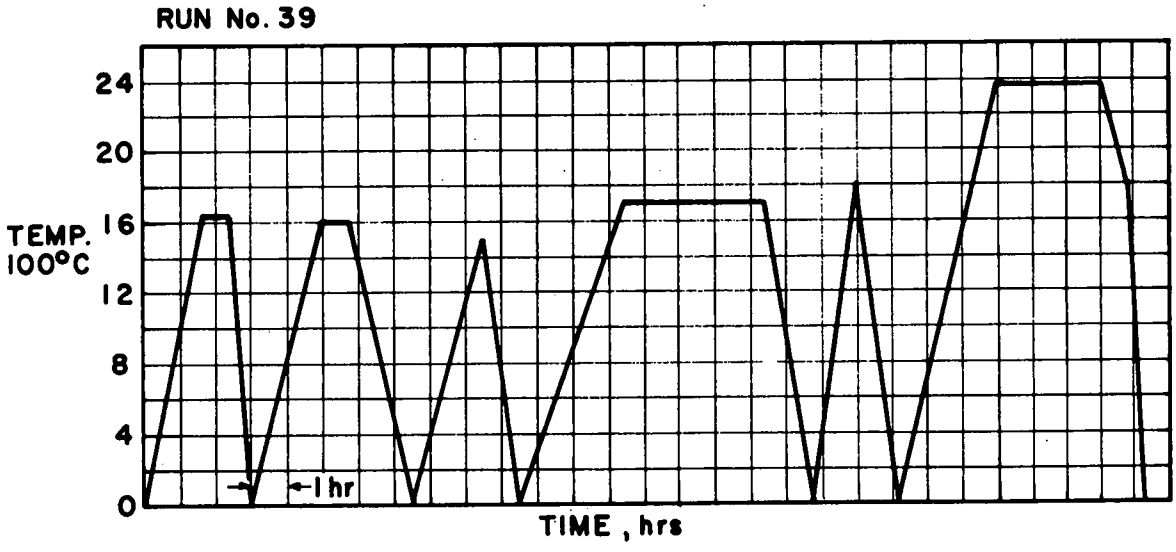

CENTERLINE TEMPERATURE HISTORY
Fig. 3

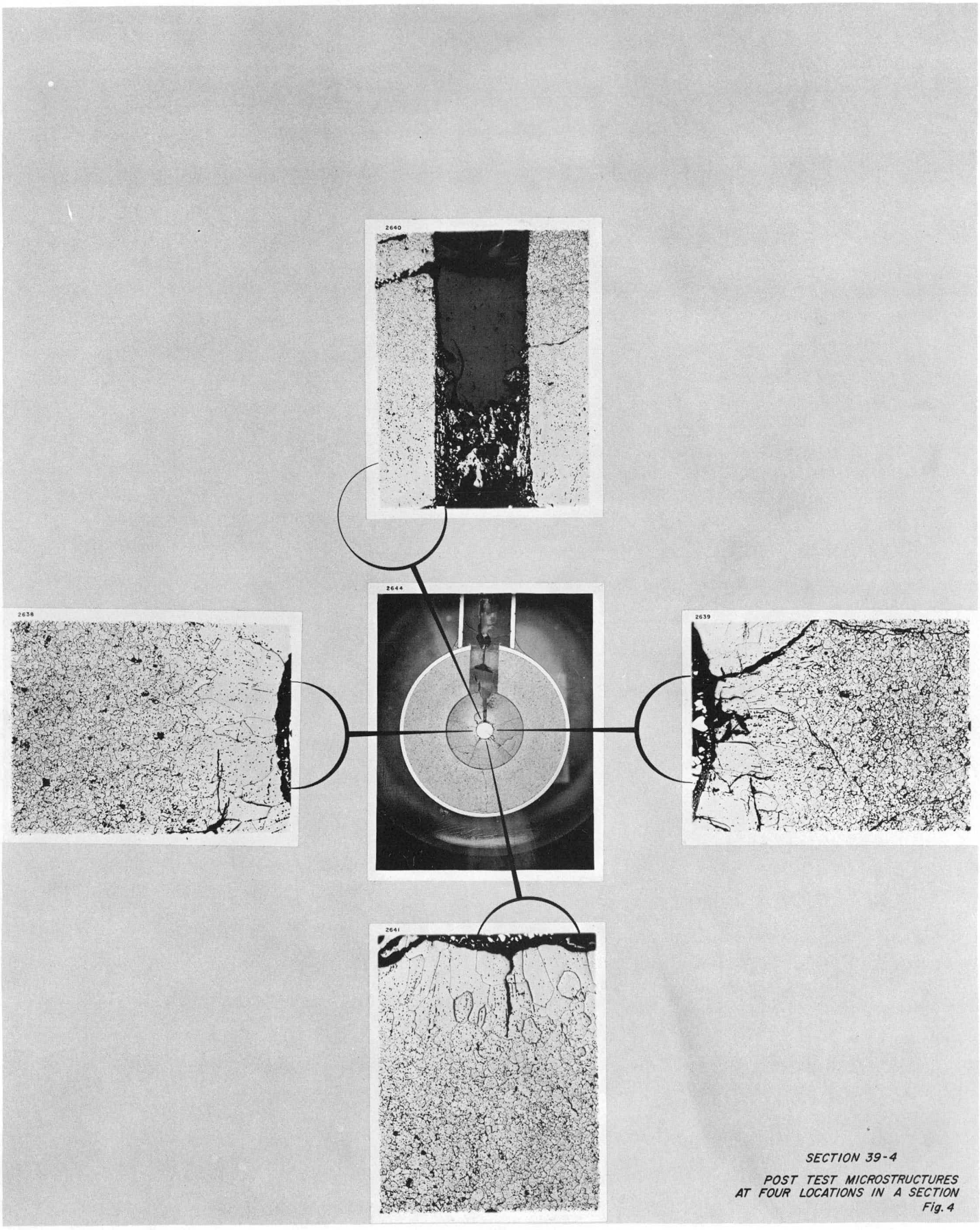

SECTION 39-4

POST TEST MICROSTRUCTURES
AT FOUR LOCATIONS IN A SECTION
Fig. 4

in size with increasing radial distance from the heater until the as-sintered grain size (approximately 10 microns diameter) was reached. Occasionally columnar grains of various sizes were encountered. These seemed to occur more frequently in element 39 (compound element with insulated pellets) than in element 38 (uninsulated pellets), but in general, were not present in all sections. Photomicrographs of typical structures from elements 38 and 39 are shown in Figures 5 and 6.

Elements 35, 36 and 37, previously reported[1], along with elements 38 and 39 were sectioned and photographed. Measurements of more than 250 photomicrographs were made to the radial distance at which onset of small equiaxed massive grains (greater than about 100 microns diameter) occurred. Element 38 was typical of the elements made from uninsulated UO_2 pellets (elements 35 to 38). Data from this element are compared with those from element 39, a compound element made from ZrO_2 insulated UO_2 pellets. Results of these measurements for elements 38 and 39 as a function of axial position are shown in Figures 7 and 8. The inside diameter of the pellet was used as the reference for measurements.

3. Temperature for Onset of Grain Growth

a. Radial Temperature Distribution

In an attempt to determine the temperature for the onset of small and massive grain growth, a radial temperature distribution for the uninsulated and insulated UO_2 elements was determined. Values from Figure 2 for thermal conductivity as a function of temperature were used and the following assumptions were made:

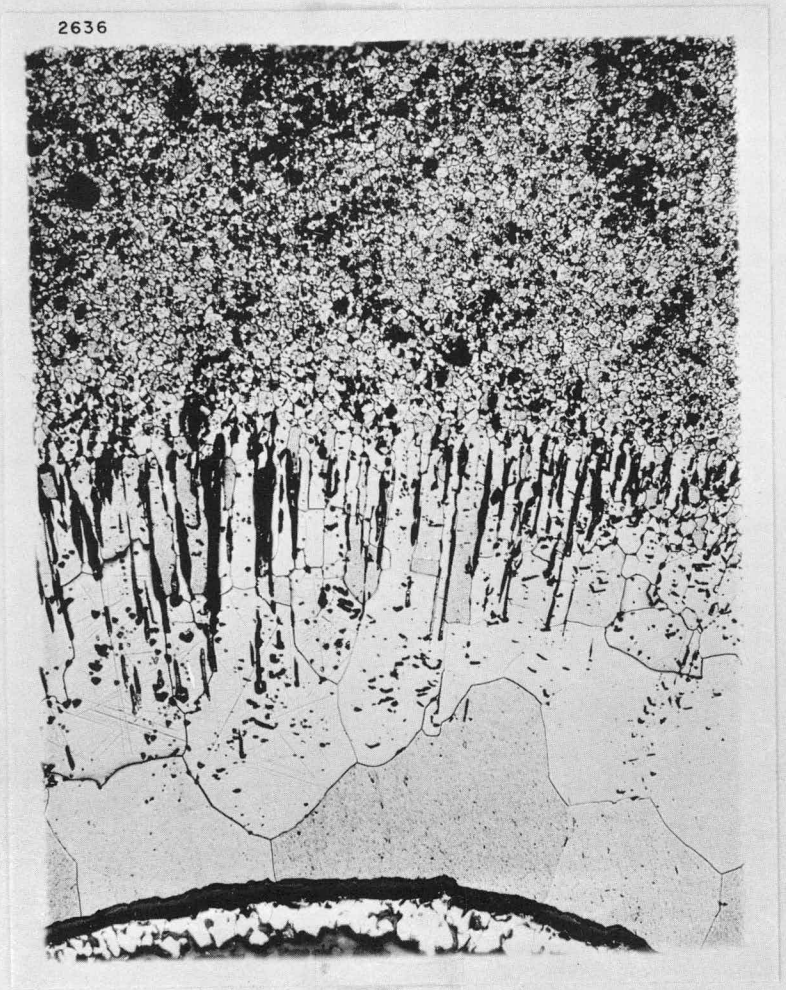

100X

SECTION 38-8

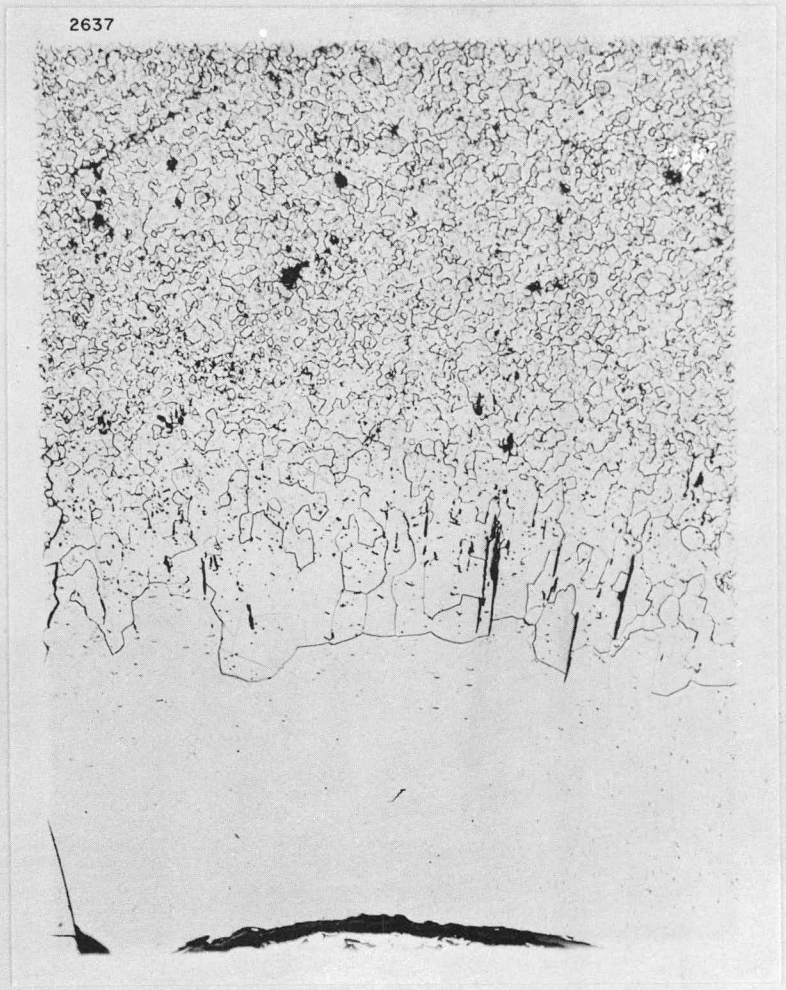

100X

SECTION 38-11

Fig. 5

POST TEST MICROSTRUCTURES - RUN No. 38

100 X

SECTION - 39-8

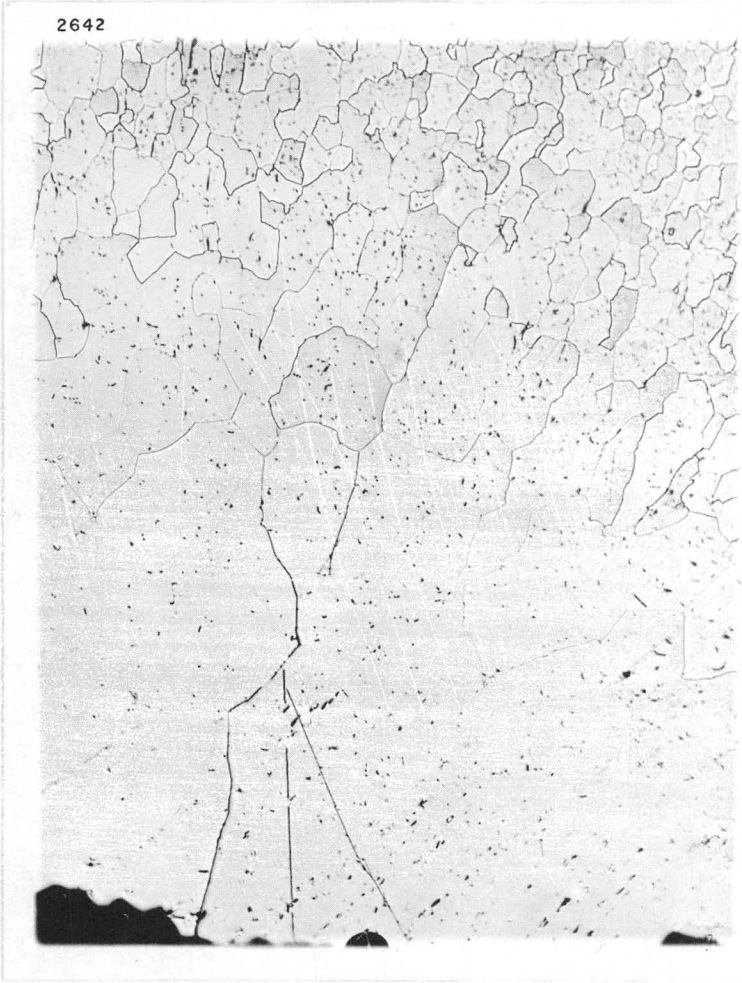

100 X

SECTION - 39-11

Fig. 6

POST TEST MICROSTRUCTURES - RUN No. 39

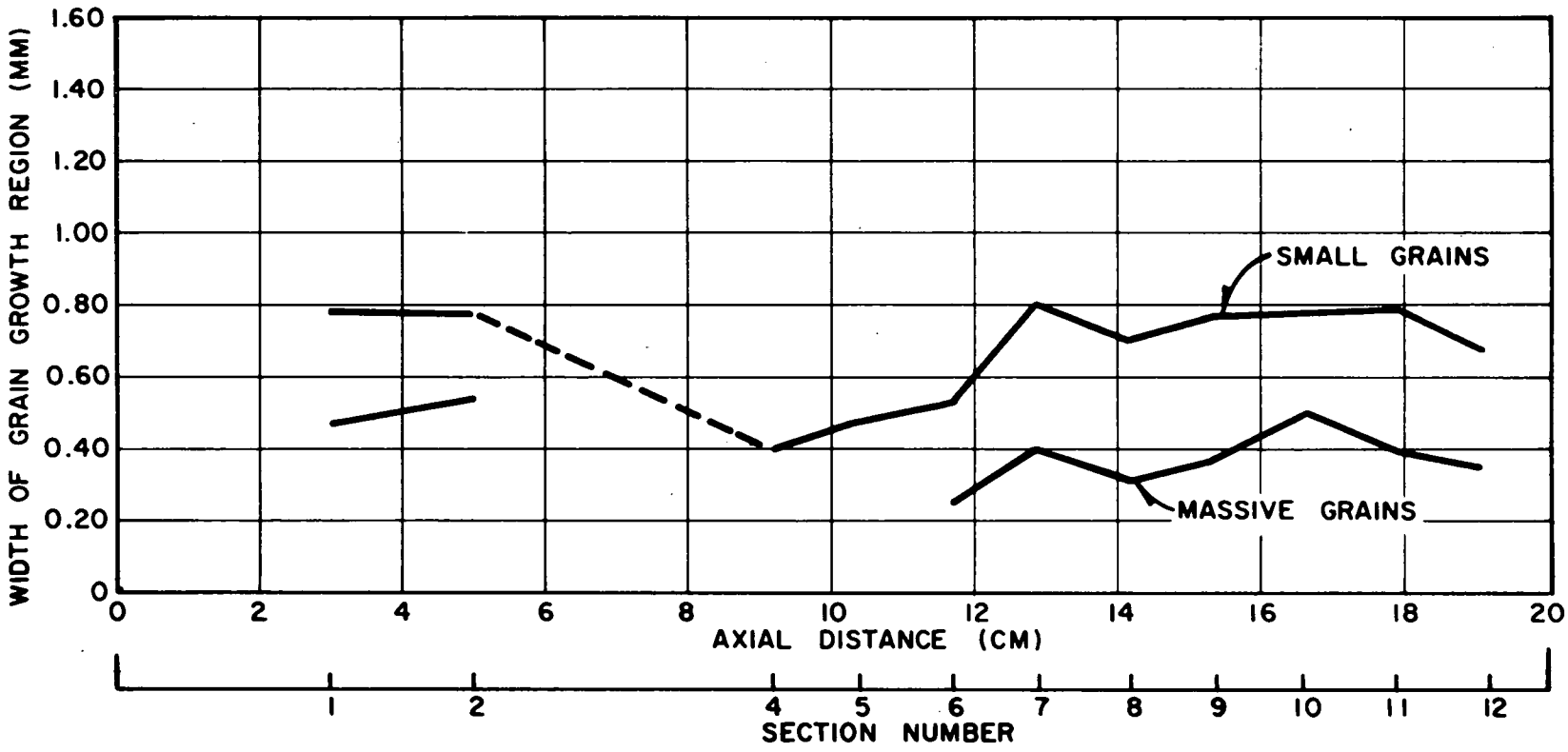

Fig. 7

RUN 38 – WIDTH OF GRAIN GROWTH REGION

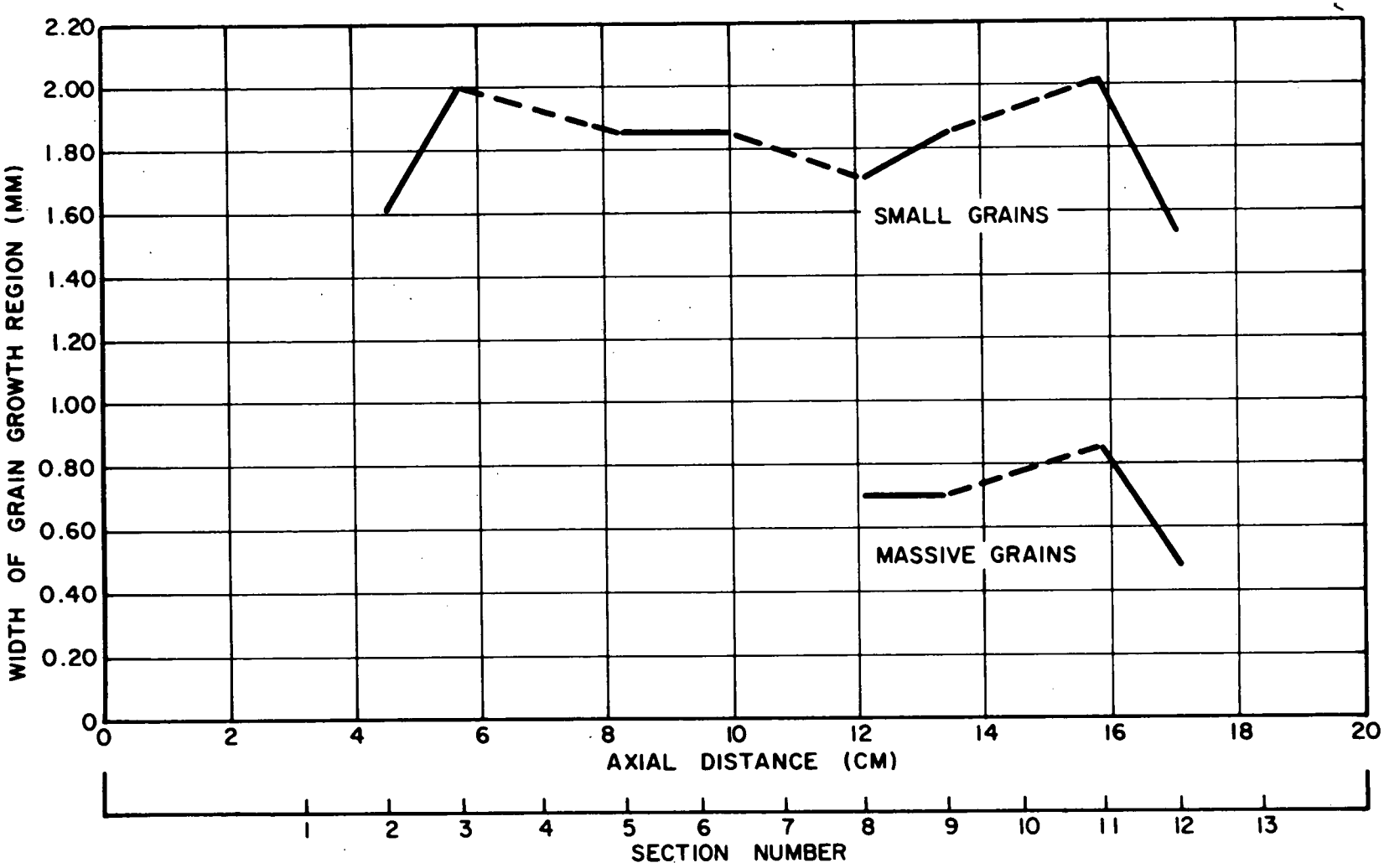

RUN 39 — WIDTH OF GRAIN GROWTH REGION

Fig. 8

(1) The UO_2 pellets were in contact with the tungsten-rhenium heater rod.*

(2) The gap (between heater rod and fuel pellet) conductance was a constant value of 2 watts/cm^2-^oC.

(3) The contribution of cracks and voids to the thermal resistance of the UO_2 was insignificant.

In addition, the outer surface of the UO_2 was assumed to be in contact with the clad for the uninsulated elements and in contact with the ZrO_2 insulator for the compound element.

Knowing the average temperature of the heater, the geometry of the element and the power required to maintain a given temperature within the element, the ID surface temperature of the UO_2 pellet was derived.

Calculations of the temperature distribution within the UO_2 pellet were made by applying the integrated form of Fourier's law for heat transmission by conduction across a homogeneous material.

$$Q = \frac{k 2\pi l \Delta T}{\ln \frac{R_2}{R_1}} \qquad (1)$$

where Q = heat flux

k = thermal conductivity

l = length of heat transfer surface

* An analysis of post-test metallography indicated, in some sections, mechanical attachment of the heater rod surface to the pellet inside diameter. In addition, there was some evidence of a change in heater rod shape resulting from heater-fuel mechanical interaction.

ΔT = temperature drop across a given segment of the material

R_1 and R_2 = radii of inner and outer surface within which a temperature drop, ΔT, occurs.

Since the heat flow across any radial segment is constant and the temperature drop is proportional to the thermal resistance of that segment, equation (1) can be put in a form from which the temperature drop across an individual radial segment can be determined.

$$\text{Thus } \Delta T_{total} = \Delta T_1 + \Delta T_2 + \Delta T_3 \ldots . \text{ etc.} \qquad (2)$$

$$\text{and } \Delta T_1 = \frac{\dfrac{\ln \frac{R_2}{R_1}}{k_{m1}}}{\dfrac{\ln \frac{R_2}{R_1}}{k_{m_1}} + \dfrac{\ln \frac{R_3}{R_2}}{k_{m_2}} + \dfrac{\ln \frac{R_4}{R_3}}{k_{m_3}} \ldots \text{ etc.}} \qquad (3)$$

where k_{m_1} = mean thermal conductivity for the average temperature of a segment having radii, R_1 and R_2, as physical boundaries.

The radial temperature distribution curves were then determined from an assumed temperature profile within a UO_2 pellet. A series of iterations were performed until the assumed radial position for a given temperature drop was identical to the calculated radial position for the same temperature drop.

The results of these operations are shown in Figure 9. It can be seen that the thermal gradient for the insulated pellets (Run 39) at any

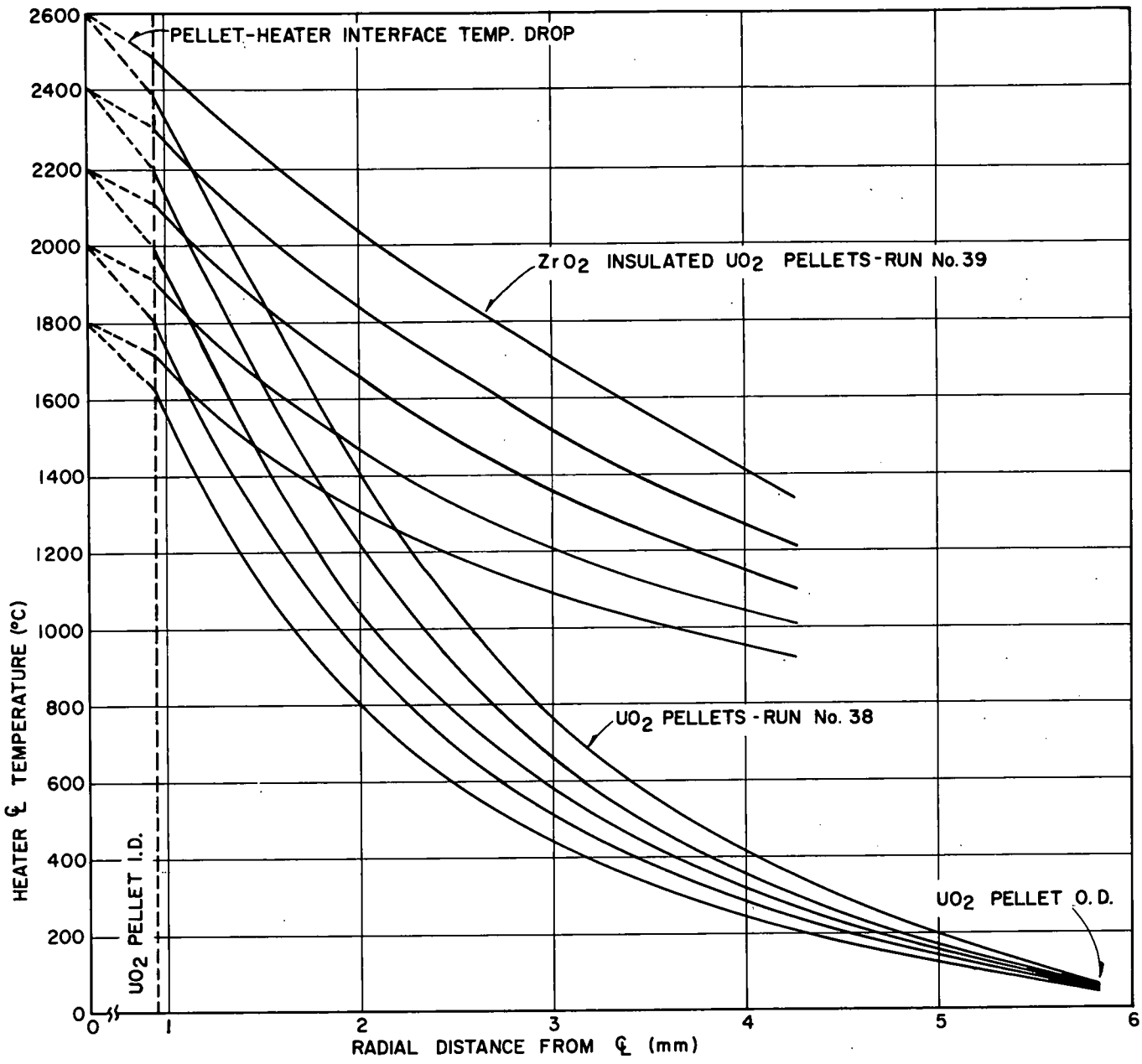

RADIAL TEMP. DISTRIBUTION - RUN No's 38 and 39

Fig. 9

point is approximately one-half the gradient in the uninsulated pellets (Run 38). The lower thermal gradient of element 39 results in higher temperatures at any given radial location within the UO_2 pellet. This gradient also more closely approximates the in-pile thermal gradient for UO_2 and, as seen in Figures 7 and 8, the grain growth region in element 39 (insulated) is about twice as wide as the grain growth region in element 38 (uninsulated). Thus, measurements of the locations of microstructural change were less difficult.

b. Determination of Temperature for Onset of Grain Growth

Using the radial temperature distribution curves (Figure 9), the measurements of distance from pellet edge to the microstructural change (Figures 7 and 8), and temperature prior to final cooldown for the section of interest, the temperature for onset of grain growth (grains with an approximate grain diameter of greater than 15 microns) and for onset of massive grains (approximate grain diameter greater than 100 microns) was determined.

The following procedure was used in determining the range of temperatures shown in Figure 12 for onset of grain growth constituents. Actual data used are shown in Table I. The optically measured temperatures (sightings to various radial positions within the UO_2) were used to enter the radial temperature distribution curves. Using the radial position of the sighting and the observed temperature for that radial position as input data (Figure 10), the intersection of these two values fell on a radial temperature profile curve from which the temperature of the pellet ID surface was obtained by following the curve back to the ordinate.

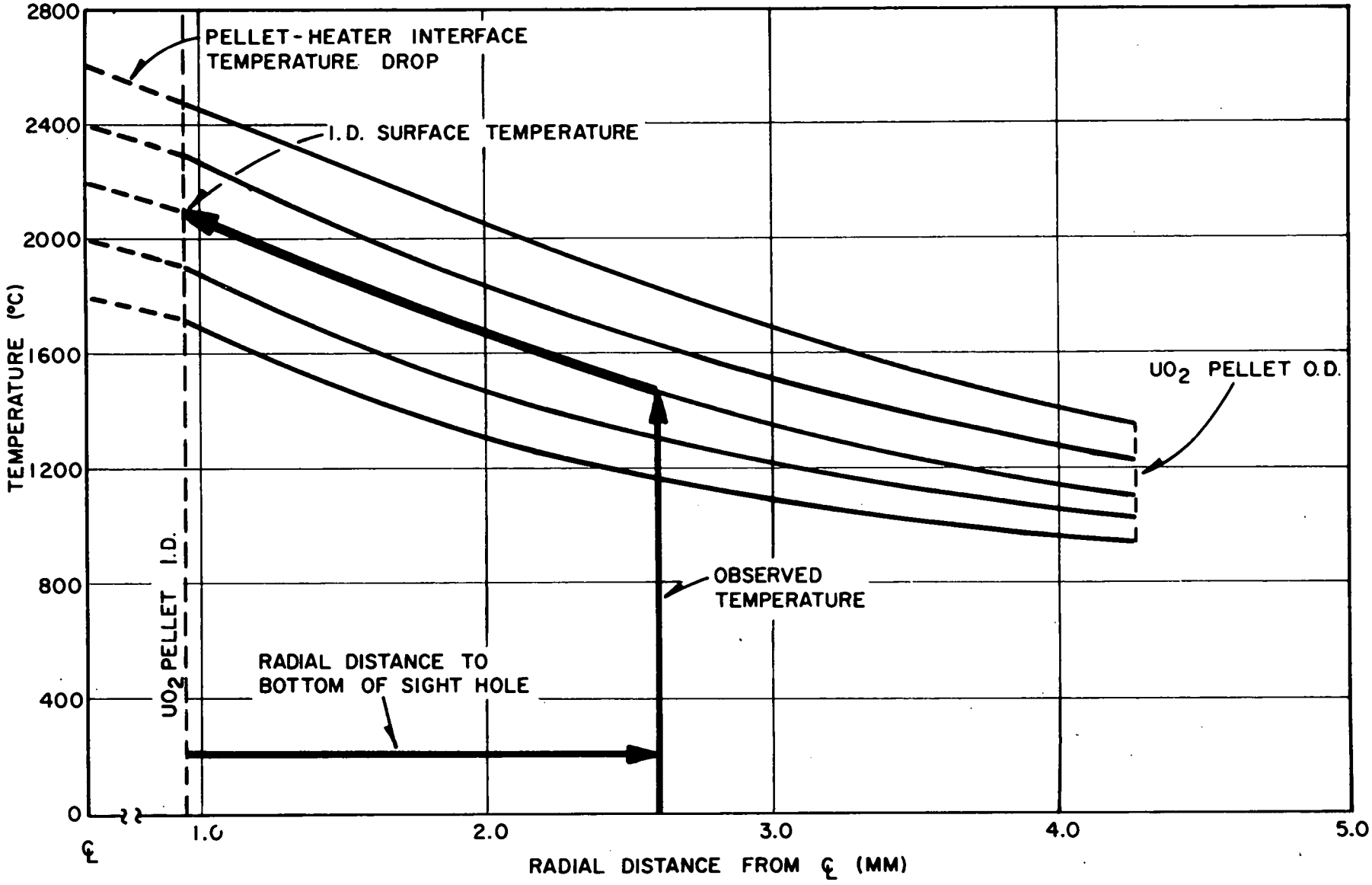

Fig. 10

TYPICAL PELLET I.D. SURFACE TEMPERATURE DETERMINATION

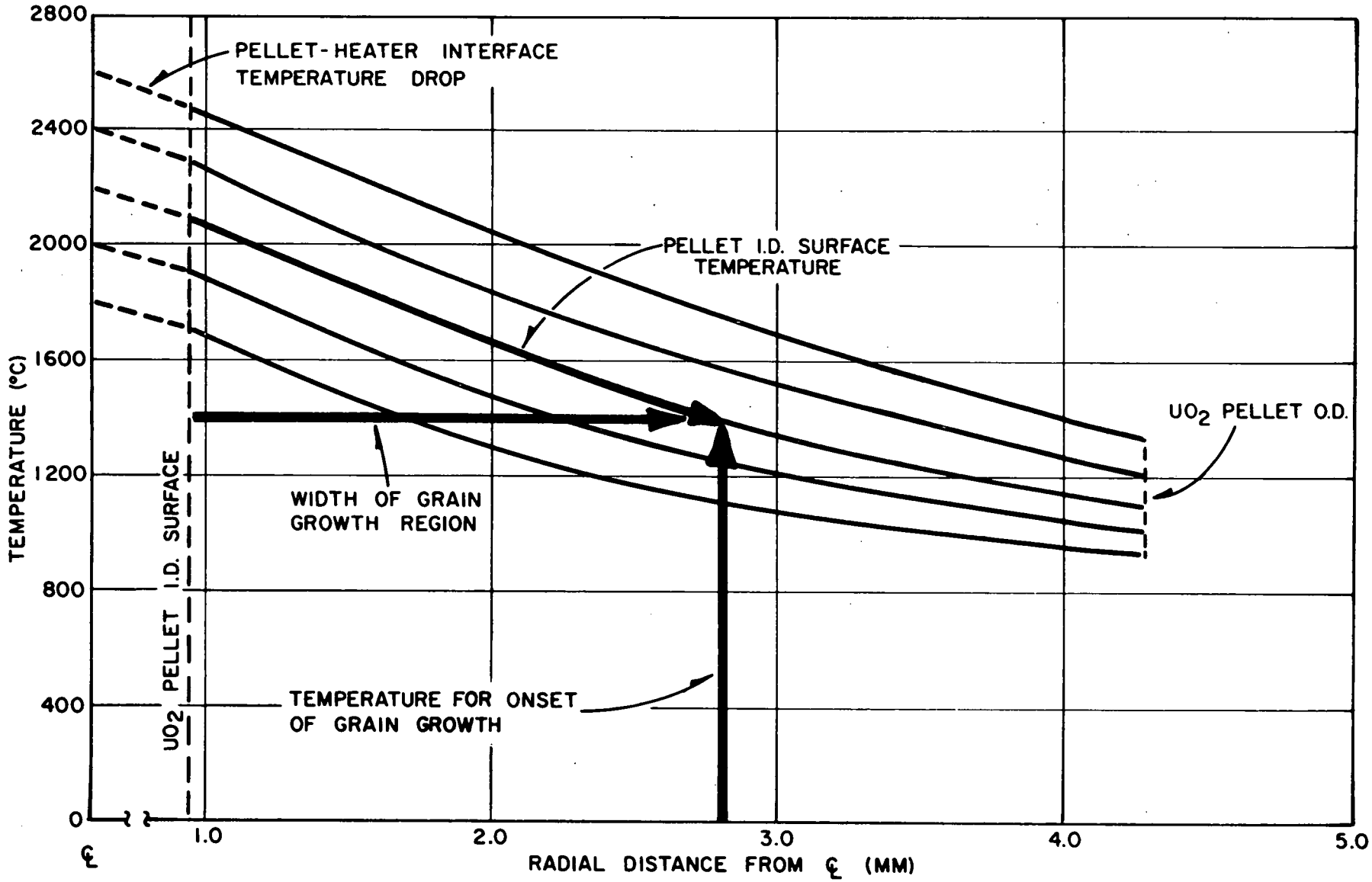

Fig. 11

TYPICAL DETERMINATION OF TEMPERATURE FOR ONSET OF GRAIN GROWTH

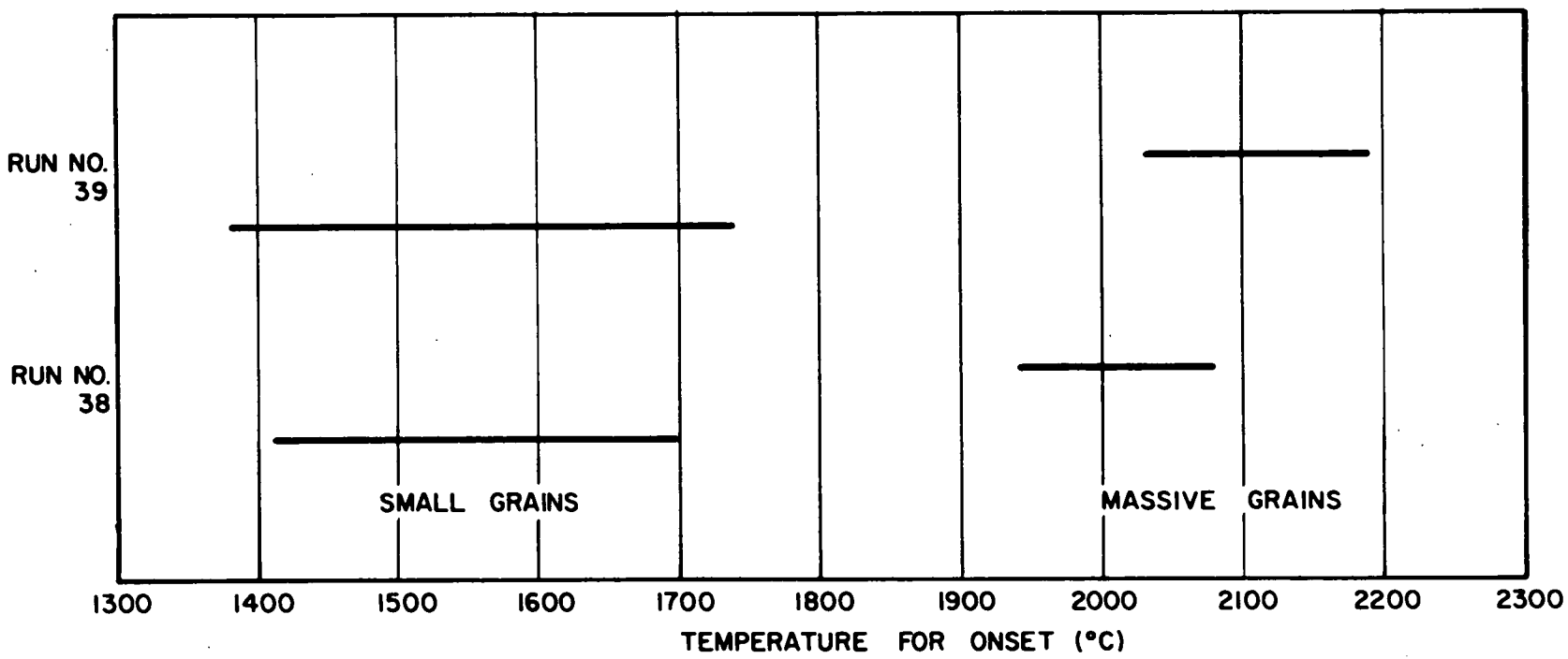

TEMPERATURE FOR ONSET OF GRAIN GROWTH

Fig. 12

TABLE I

TEMPERATURE FOR ONSET OF GRAIN GROWTH

	Sighthole Number	Section Number	Dist. from ℄ to Bottom of Sighthole (mm)	Observed Temperature (°C)	Dist. from Pellet ID to Grain Size Change (mm)		Temperature for Onset (°C)	
					Small Grains	Massive Grains	Small Grains	Massive Grains
RUN 38	6	4	1.97	956	0.40	--	1410	--
	9	7	2.60	1060	0.80	0.40	1700	2080
	12	10	1.97	1485	0.78	0.50	1680	1940
RUN 39	2	2	4.27	1176	1.61	--	1610	--
	3	3	2.96	1460	2.00	--	1460	--
	5	5	1.69	1740	1.85	--	1380	--
	6	6	4.27	1068	1.85	--	1380	--
	8	8	1.69	2011	1.70	0.70	1680	2030
	9	9	2.96	1690	1.85	0.70	1740	2150
	11	11	4.27	1411	2.15	0.85	1740	2190

This temperature determined a specific temperature profile within the pellet. The temperature of onset of a particular microstructure was determined by moving along the temperature profile curve determined by the pellet ID surface temperature for the section (Figure 11), to the intersection of the measured radial distance for the microstructure of interest. The intersection of these two values established the temperature for onset of the microstructure of interest.

Figure 12 shows that the temperature range for onset of grain growth for the UO_2 in the uninsulated (element 38) and insulated (element 39) elements are approximately the same, the range for the former element being slightly narrower. The temperature range for onset of massive grains appears to be lower in the element with the higher temperature gradient, although overlap of data exists.

D. Conclusions

It is concluded that the thermal conductivity of sintered UO_2 pellets decreases with temperature to a value between 0.025 and 0.033 watts/cm^2-^oC at about 1400^oC and then rises to about 0.034 to 0.046 watts/cm^2-^oC at 2000^oC and 0.048 to 0.059 watts/cm^2-^oC at 2400^oC. These results, compared to the low temperature results reported by Daniel[2] et al, and Godfrey[3] et al, show reasonable agreement at around 1000^oC. At higher temperatures, the shape of the CEND conductivity versus temperature curve is similar to that reported by Feith[5], although the increase in conductivity with temperature after passing through a minimum is greater for the CEND data.

It was found that grain growth initiated at temperatures in the range of 1400 to 1700^oC and that growth of massive grains occurred at temperatures

around 2000°C. A trend toward lower temperatures for the onset of massive grain growth was observed at higher thermal gradients, although overlap in the data existed. The temperature ranges reported for the onset of small and massive grain growth are important benchmarks for post-irradiation evaluation of UO_2 irradiations under typical present-day power reactor conditions where the specific power in the element is not sufficient to produce large columnar grains or melting.

E. Future Work

An additional element of the compound (element 39) configuration will be tested in an attempt to verify the shape and position of the thermal conductivity curves and to more closely establish the temperature for onset of grain growth. The latter objective will be achieved by providing more sight holes in the UO_2 at radial positions near those calculated for the onset of microstructural constituents.

III. COLLAPSE CRITERIA

E. I. Veil

A. Introduction

In previous work at CEND the Tangent Modulus Criterion closely approximated the collapse pressure in stainless steel tubing with diameters up to 1.9 cm (0.750 in.) and tube thickness to radius ratios (t/R) up to 0.012. The present program was initiated to determine whether this criterion can be applied to tubing with diameters up to 3.175 cm (1.250 in.). Type 347 weldrawn annealed tubing, 3.175 cm (1.250 in.) in outside diameter with six different wall thicknesses in the range of 0.07 to 0.19 cm (0.028 to 0.075 in.) was procured for this investigation. The experimental effort and results are discussed below.

B. Experimental Effort

Two collapse test specimens were fabricated for each of the six different wall thicknesses (0.028 to 0.075 in.) of the 3.175 cm diameter tubing. The specimens were 63.5 cm in length which represented a length to diameter ratio of 20. The collapse data are shown in Table II.

Figure 13 is a plot of the actual collapse pressure versus the predicted collapse pressure for the Tangent Modulus, Elastic, and Inelastic Criteria. In this Figure the solid line indicates complete agreement between actual and predicted values; a range of $\pm 20\%$ from this line is also shown. In using the Tangent Modulus Criterion, the value of Poisson's ratio was set as a function of the tangent modulus (E_t), since Poisson's ratio is greater for plastic deformation than for elastic strain. As E_t decreased, Poisson's ratio increased from 0.3 to 0.5 as indicated in Table III.

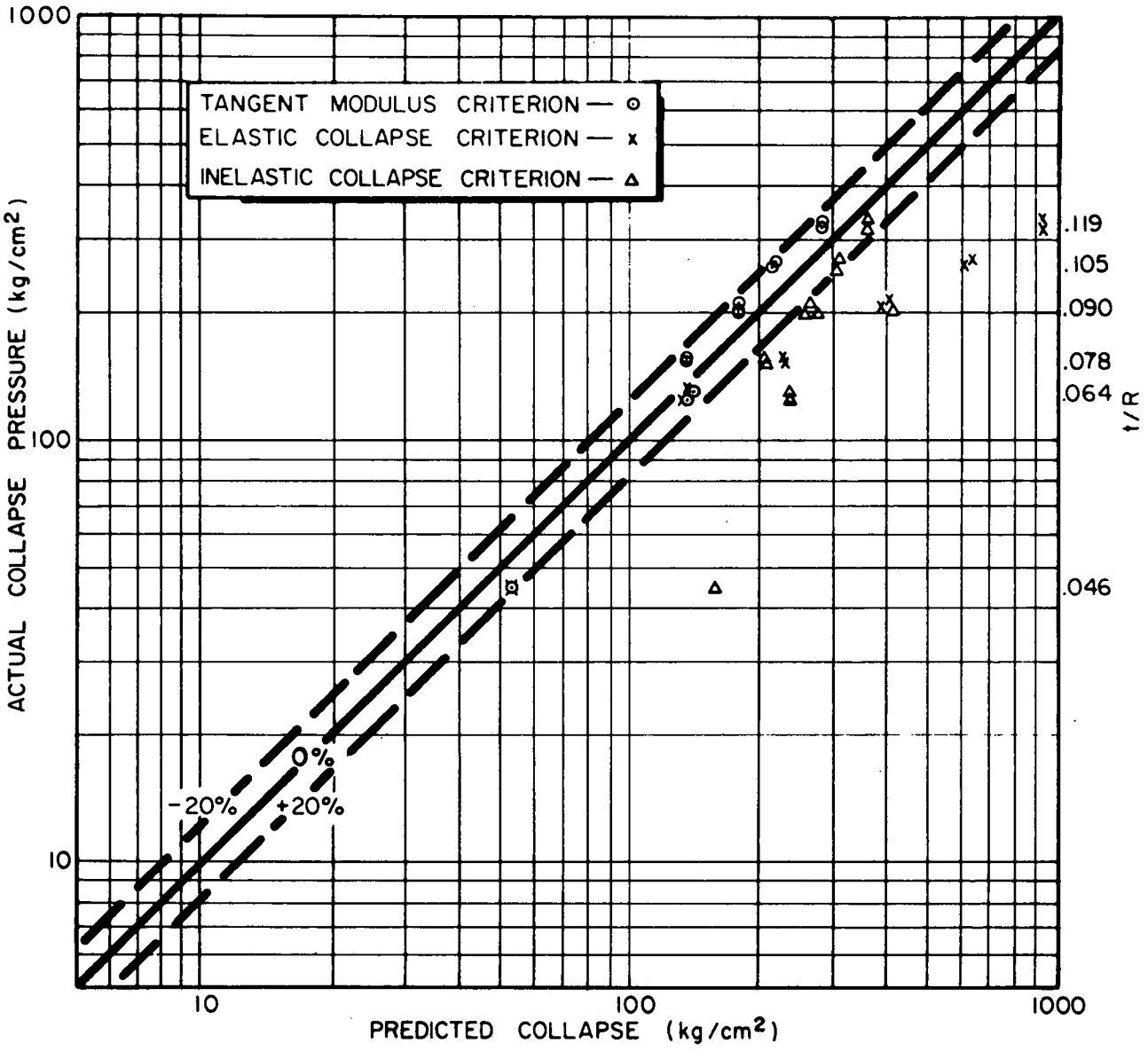

VARIATION OF ACTUAL FROM PREDICTED ROOM TEMPERATURE COLLAPSE VALUES FOR 3.175 Cm. ANNEALED TUBING

Fig. 13

TABLE II - Collapse Data

Sample No.	Material	Avg. Wall Thickness (cm)	Avg. OD (cm)	t/R_o [a]	Ovality [b]	Avg. 0.2% Offset Y.S. (kg/cm^2)	Actual Collapse Pressure (kg/cm^2)	Collapse by Tangent Modulus [c] (kg/cm^2)	Predicted Collapse by Elastic Criterion [d] (kg/cm^2)	Predicted Collapse by Inelastic Criterion [e] (kg/cm^2)	Actual Collapse Pressure Normalized to 2660 (kg/cm^2)
CT-A-28-1	347	.073	3.177	.046	.10	3197	45.5	53.2	53.2	154.5	(f)
CT-A-28-2	347	.072	3.175	.045	.10	3197	44.8	53.2	53.2	154.5	(f)
CT-A-40-1	347	.101	3.172	.064	.04	3358	131.3	139.7	135.5	232.1	104.0
CT-A-40-2	347	.101	3.172	.064	.04	3358	127.8	139.7	135.5	232.1	101.2
CT-A-49-1	347	.123	3.177	.078	.20	2511	157.5	135.1	225.3	202.1	166.8
CT-A-49-2	347	.124	3.176	.078	.28	2511	155.8	135.1	225.3	200.7	165.0
CT-A-56-1	347	.144	3.178	.091	.04	2688	211.8	176.8	404.3	263.4	209.7
CT-A-56-2	347	.143	3.176	.090	.10	2688	199.5	175.0	391.0	256.3	197.5
CT-A-56-3	347	.143	3.176	.090	.02	2688	204.8	175.0	391.4	265.6	202.8
CT-A-65-1	347	.166	3.175	.105	.02	2657	266.0	213.5	619.2	303.1	266.0
CT-A-65-2	347	.166	3.176	.104	.06	2657	264.3	211.1	601.7	297.2	264.3
CT-A-75-1	347	.188	3.170	.119	.04	2717	329.0	274.8	904.4	347.8	322.1
CT-A-75-2	347	.188	3.171	.119	.06	2717	325.5	274.8	904.4	343.3	318.7

(a) t/R_o = Average wall thickness ÷ Radius.

(b) Dmax - Dmin/Dmin · 100%; where D = Outside diameter.

(c) $P_c = \frac{E_t}{4(1 - a^2)} (t/R_o)^3$; E_t = Tangent Modulus, a = Poisson's Ratio

Reference: "The Development and Testing of UO_2 Fuel Systems for Water Reactor Applications," CEND-157, June 1962.

(d) $P_c = \frac{E}{4(1 - a^2)} (t/R_o)^3$; where a = 0.284, and E = Young's Modulus.

(e) $P_c = \frac{(1 - B)\ \sigma y\ (1 - R_i^2/R_o^2)}{\sqrt{3}}$; where B = Percentage reduction in collapse strength due to out-of-roundness.
σy = 0.2% offset yield strength of the material.
R_i = Inside radius.

(f) Collapse is elastic, therefore, independent of yield strength in this range.

TABLE III

Variation of Poisson's Ratio With Tangent Modulus

Poisson's Ratio	Tangent Modulus (10^4 kg/cm^2)
0.30	210
0.315	203
0.33	196
0.345	189
0.36	182
0.37	175
0.38	168
0.39	161
0.40	154
0.41	147
0.42	140
0.43	133
0.44	126
0.45	119
0.475	112
0.50	7 - 105

The following conclusions were based upon data presented in Figure 13.

1. With the exception of data points represented by the Tangent Modulus Criterion, all data fell below the indicated straight line relationship between actual and predicted collapse pressures. Thus, collapse pressures predicted by either the Elastic or Inelastic Collapse Criteria are greater than those actually observed.

2. For the range of t/R investigated, data points represented by the Tangent Modulus Criterion consistently fell within the band of $\pm 20\%$ surrounding the indicated straight line relationship. With one major exception at a t/R of 0.046, all deviations from the solid line were in the direction of larger measured collapse pressures than those calculated. Thus, values obtained through application of the Tangent Modulus Criterion are considered to be conservative.

3. The Elastic Criterion provides a reasonably close relationship between actual and predicted collapse up to a t/R of 0.060. As anticipated (see Figure 14) in the region beyond the transition between Elastic and Inelastic behavior, the Inelastic Criterion becomes more accurate at t/R is increased.

4. Except for the range of t/R from 0.060 to 0.115*, the combined use of the Elastic and Inelastic Criteria, in which the lowest calculated collapse pressure is employed, provides a reasonably accurate prediction of actual collapse pressures. However, as noted above, all deviations are in the direction of predicting lower than actual collapse pressures.

* By extrapolation from Figure 14.

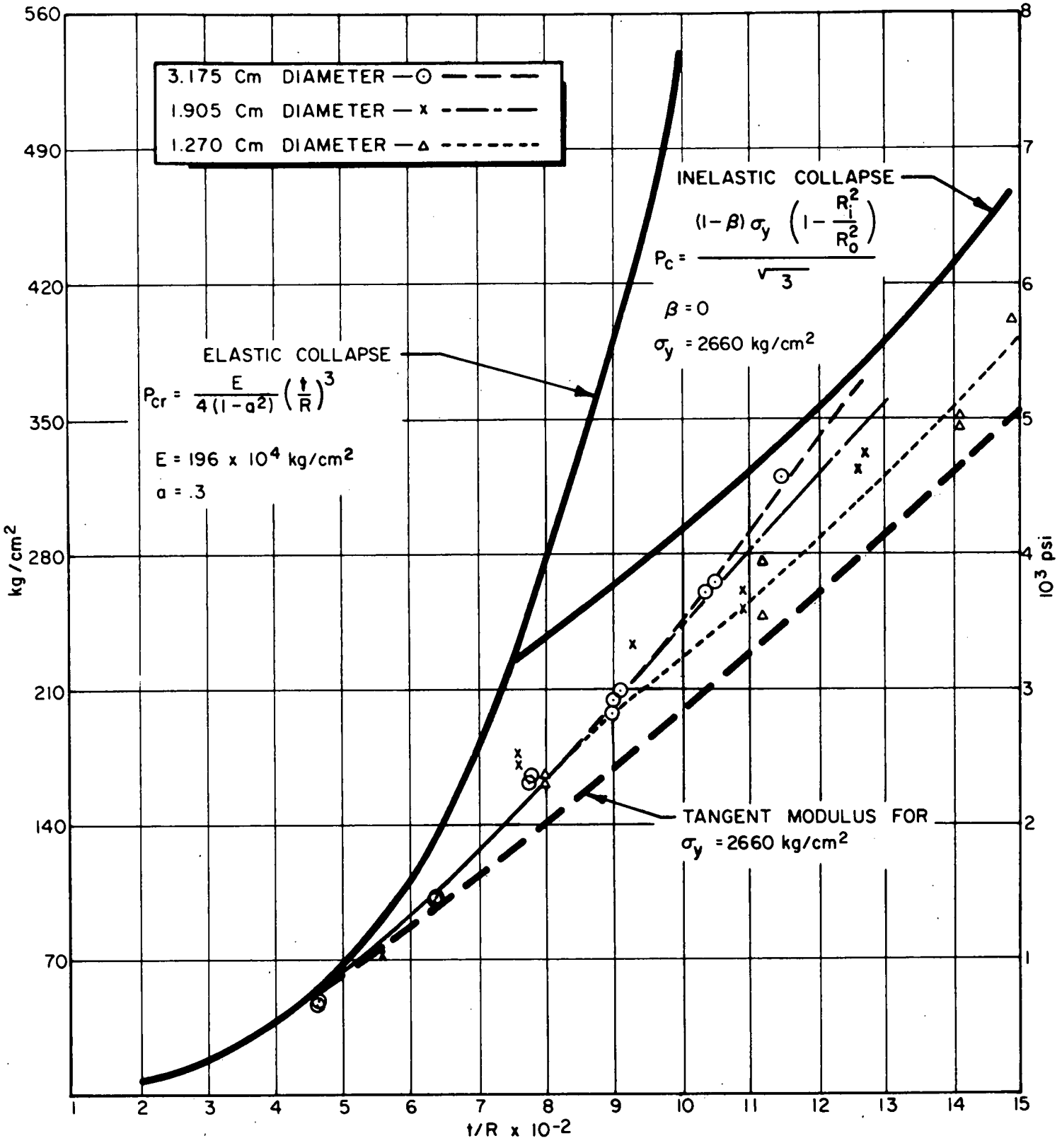

COLLAPSE OF ANNEALED STAINLESS STEEL TUBES AT ROOM TEMPERATURE

Fig. 14

5. For the entire range of t/R investigated, the Tangent Modulus Criterion provides the most conservative estimate of collapse pressures. In all cases the difference between actual and predicted collapse, using this Criterion, was less than 20%.

Figure 14 shows a plot of the collapse pressures for the room temperature 3.175 cm outside diameter annealed tubing normalized to a yield strength of 2660 kg/cm^2 (38,000 psi) as a function of t/R_o (thickness to outside radius). Included for comparison, are data points generated on an earlier program[6,7] for 1.270 and 1.905 cm (0.500 and 0.750 in.) outside diameter annealed tubing. Data points were not corrected for ovality since the influence of ovality on tube collapse was not observed until the ovality exceeded 1% in 1.270 and 1.905 cm diameter tubing and 0.3% in 3.175 cm tubing. (The greatest ovality observed in the 3.175 cm tubing was 0.3%.) Also plotted are the predicted collapse curves based on the three collapse criteria.

Data shown in Figure 14 not only substantiate the conclusions made above for the 3.175 cm diameter tubing, but also indicates that these conclusions are generally applicable to the range of tube diameters investigated. The Tangent Modulus Criterion provides a close approximation of actual collapse for the 1.270 cm diameter tubing. As the tube diameter increases, there is poorer agreement between actual collapse pressures and those predicted from the Tangent Modulus Criterion. As the cladding diameter increases, actual collapse pressures approach those predicted by the Inelastic Model at lower t/R values. With only one exception (t/R = 0.046), all measured collapse pressures fell below those predicted by either the Elastic or Inelastic Collapse Criteria. On the other hand, the Tangent Modulus Criterion provided

a reasonably accurate, but conservative, indication of collapse pressure; the agreement for the smaller tubing (typical of boiling- and pressurized-water cladding) was particularly good.

IV. PROJECTION WELDING

G. Zuromsky

A. Introduction

This task has the following objectives:

1. To refine the projection welding method for the fabrication of 61-tube hexagonal clusters, 7 feet in length, of Type 347 stainless steel and Zircaloy-2. The feasibility of the method was established earlier in this program.

2. To test and evaluate full size clusters fabricated from the two materials for differential thermal expansion behavior to establish overall structural soundness and dimensional integrity of the weldments.

Current program activity has centered on improvements in the fabrication process to develop optimum quality tube-to-spacer wire welds and closer dimensional control of tube-to-tube spacings. Further modifications were made in electrode tooling and cluster fixturing with emphasis on control of alignment and positions of assembled tubes during welding.

B. Experimental Effort

Two additional subassemblies, each consisting of two rows of eight and nine tubes of Type 347 stainless steel, were fabricated at Sciaky Brothers, Inc. and evaluated at CEND. The tubes were 1.2700 cm $\pm$0.0013 cm (0.5000 $\pm$0.0005 inch) diameter by 0.051 $\pm$0.005 cm (0.020 $\pm$0.002 inch) wall thickness and 45.7 cm (18 inches) in length. The spacer wires joining the two rows of tubes were 0.1575 $\pm$0.0013 cm (0.0620 $\pm$0.0005 inch) in diameter. Both materials were in the bright annealed condition.

The results of dimensional measurements of tube center-to-tube center distances are included in Table IV. The inspection data show that distances between adjacent tubes in both rows of the two subassemblies were maintained within the required range of 1.587 $\pm$0.008 cm (0.625 $\pm$0.003 inch). Spacings for the end tubes on both sides of the second subassembly were out of specification. Cross wires had not been welded to the outside of this subassembly and it is probable that the unrestrained side tubes may have rolled during shipment.

Lateral displacement or skewing between rows of tubes, reported for previous subassemblies[1], has been essentially eliminated by further improvements in fixturing of rows of tubes. However, the diagonal spacing between adjacent tubes was consistently on the high side of the nominal dimension of 1.587 cm (0.625 inch). This diagonal tube center to tube center spacing may be expressed as follows from data of Table IV.

Spacings at one end	$1.597\ ^{+0.005}_{-0.003}$ cm or $0.629\ ^{+0.002}_{-0.001}$ inch
Spacings at opposite end	$1.597\ ^{+0.010}_{-0.003}$ cm or $0.629\ ^{+0.004}_{-0.001}$ inch

In order to attain the desired 1.587 $\pm$0.008 cm (0.620 $\pm$0.003 inch) dimension, a reduction of about 0.010 cm (0.004 inch) is required in the spacing between tube rows. This will be accomplished by increasing the spacer wire setdown, i.e., reduction in the diameter of the spacer wire at the tube-spacer wire joints as a result of weld metal expulsion. Spacer wire setdown for these evaluation subassemblies has been limited to 0.015 cm (0.006 inch) for all

TABLE IV - Dimensional Inspection of Tube-to-Tube Spacings

		First Subassembly	Second Subassembly
TUBES WITHIN ROWS			
One End	8-tube row	$1.587\ ^{+0.008}_{-0.008}$ cm ($0.625\ ^{+0.003}_{-0.003}$ inch)	$1.587\ ^{+0.000}_{-0.008}$ cm ($0.625\ ^{+0.000}_{-0.003}$ inch)
	9-tube row	$1.587\ ^{+0.003}_{-0.008}$ cm ($0.625\ ^{+0.001}_{-0.003}$ inch)	$1.587\ ^{+0.003}_{-0.008}$ cm ($0.625\ ^{+0.001}_{-0.003}$ inch)
Opposite End	8-tube row	$1.587\ ^{+0.003}_{-0.008}$ cm ($0.625\ ^{+0.001}_{-0.003}$ inch)	$1.587\ ^{+0.000}_{-0.008}$ cm ($0.625\ ^{+0.000}_{-0.003}$ inch)
	9-tube row	$1.587\ ^{+0.003}_{-0.003}$ cm ($0.625\ ^{+0.001}_{-0.001}$ inch)	$1.587\ ^{+0.008}_{-0.008}$ cm ($0.625\ ^{+0.003}_{-0.003}$ inch)
TUBES BETWEEN ROWS (DIAGONAL SPACINGS)			
One End		$1.587\ ^{+0.020}_{-0.005}$ cm ($0.625\ ^{+0.008}_{-0.002}$ inch)	$1.587\ ^{+0.020}_{-0.000}$ cm ($0.625\ ^{+0.008}_{-0.000}$ inch)
Opposite End		$1.587\ ^{+0.033}_{-0.003}$ cm ($0.625\ ^{+0.013}_{-0.001}$ inch)	$1.587\ ^{+0.015}_{-0.000}$ cm ($0.625\ ^{+0.006}_{-0.000}$ inch)

joints. Earlier work on the program had demonstrated that setdown of 0.020 cm (0.008 inch) had produced welds of suitable quality. Thus, an increase in spacer wire setdown from 0.015 to 0.020 cm should reduce the spacing between tube rows by 0.010 cm without seriously affecting weld quality.

A final 2-row, 17-tube subassembly of Type 347 stainless steel will be welded and evaluated to demonstrate the capability of the fabrication process to provide the required dimensional and structural integrity.

C. Thermal Tests

Upon complete verification of the projection welding process, a 61-tube hexagonal cluster, 7 feet in length, will be fabricated from Type 347 stainless steel. This cluster will represent the highest attainable quality welds as well as control of tube-to-tube dimensions to within $\pm$0.008 cm of the nominal value of 1.587 cm. The cluster will be tested to demonstrate the ability of spacer wires to accommodate differential thermal expansion of adjacent tubes without causing failures at the tube-spacer wire joints. Performance capability will be determined by pre-test and post-test evaluations involving dimensional measurements, metallographic and mechanical tests (tensile and shear) of selected welds.

All of the components required to assemble the apparatus for the differential thermal elongation tests have been either fabricated or purchased. Modifications have been incorporated which will ensure free relative motion of tubes within the manifolds. The system contains hot and cold water lines which are channeled alternately through rows of tubes of the test assembly. These tests will evaluate the capability of full scale clusters, fabricated from Type 347 stainless steel and Zircaloy-2, to withstand cyclic temperature

changes of 10°C (20°F) between rows of tubes for 3000 temperature reversals.

D. Future Work

The final phase of the program includes the fabrication of two 61-tube hexagonal clusters, 2.13 meters (7 feet) in length, of Type 347 stainless steel and Zircaloy-2. The Zircaloy cluster will be projection welded in an inert atmosphere. Both clusters will be similarly tested for differential thermal expansion behavior. Post-test evaluations will establish the overall structural soundness and dimensional integrity of the clusters.

REFERENCES

1. Chernock, W. P., Burdg, C. E., Veil, E. I., and Zuromsky, G., CEND-2863-211 (March 1964), "The Development and Testing of UO_2 Fuel Systems for Water Reactor Applications - Progress Report."

2. Daniel, J. L., Matolick, J., Jr., and Deem, H. W., "Thermal Conductivity of UO_2," USAEC Report HW-69945, p. 3, Hanford Laboratories, September 1962.

3. Godfrey, T. G., Fulkerson, W., Kollie, T. G., Moore, J. P., McElroy, D. L., "Thermal Conductivity of Uranium Dioxide and Armco Iron by Improved Radial Heat Flow Technique," USAEC Report ORNL-3556, pp. 16-17, Oak Ridge National Laboratory, June 1964.

4. de Halas, D. R., Understanding UO_2 Thermal Conductivity, "Nucleonics," 21, No. 10, 92, 1963.

5. Feith, A. D., "Thermal Conductivity of UO_2 by a Radial Heat Flow Method," Report TM-63-9-5, General Electric Company.

6. Chernock, W. P. and Murtha, B. E., CEND-157 (June 1962), "The Development and Testing of UO_2 Fuel Systems for Water Reactor Applications - Summary Report."

7. Chernock, W. P., Burdg, C. E., Andrews, M. G., Veil, E. I., and Mordarski, W. J., CEND-199 (September 1963), "The Development and Testing of UO_2 Fuel Systems for Water Reactor Applications - Progress Report."